NUCLEAR INSTRUMENTS AND METHODS 105 (1972) 573–584; © NORTH-HOLLAND PUBLISHING CO.

ACCURATE MEASUREMENT OF THE COUNTING EFFICIENCY OF A NE-213 NEUTRON DETECTOR BETWEEN 2 AND 26 MeV*

M. DROSG†

Los Alamos Scientific Laboratory, University of California, Los Alamos, New Mexico 87544, U.S.A.

Received 4 July 1972

The neutron detection efficiency of a liquid scintillator (NE-213, 12 cm diam. × 5.7 cm) was measured with various bias settings corresponding to proton energies from 1 MeV to 6 MeV. For neutron energies below about 12 MeV a simplified calculation fits the data very well and the uncertainty in the shape is less than 2%. The importance of contributions from the reaction $^{12}C(n,n')3\alpha$ above that energy is shown. An extensive survey of publications dealing with the efficiency of organic scintillators is also presented.

1. Introduction

The quality of angular distribution measurements of neutrons with the time-of-flight method depends strongly on the precise knowledge of the energy dependence of the neutron detection efficiency, especially when light nuclei are involved (see, e.g., ref. 1). Organic scintillators[2,3]) are generally used in the measurements. Because of the generally high γ background recorded by these detectors, n–γ discrimination[4]) should be used. Liquid scintillators have better discrimination properties[5]); therefore they are very often the best choice.

Previous publications on efficiency measurements dealt either with energies below 5 or 10 MeV or with very high energies up to 390 MeV (see table 1). Below about 12 or 14 MeV (depending on the pulse-height bias and the type of scintillator), the measurements and even simplified calculations agree very well. For the higher energies, agreement within 10% between measured points and calculations is generally achieved.

In fast neutron scattering, as done at the time-of-flight facilities of the Los Alamos Scientific Laboratory (LASL), the knowledge of the energy dependence of the efficiency (relative efficiency) is one of the limiting factors. Energies up to about 23 MeV are measured. Few published efficiency curves extend above 14 MeV, and these are either of low statistical quality[6]) or are based on a few points between 14 MeV and 30 MeV[7–14]). Further, as will be discussed later, these curves cannot be applied to a detector of different size or with a different scintillator.

Calculations in this range suffer from complications due to the reaction $^{12}C(n,n')3\alpha$ which is, therefore, often not taken into account[6,15–18]) despite its known importance[7,10,13,19–23]). To determine the efficiency in this energy range with sufficient confidence, a precise measurement seems to be the best solution. Thus, the pronounced contribution from the reaction $^{12}C(n,n')3\alpha$ can best be accounted for.

In this work the efficiency was derived by comparing the yields of $^1H(n,n)^1H$ angular distribution measurements with the corresponding differential cross sections.

2. Survey of efficiency determinations

The difficulties in calculating the detection efficiency for neutrons arise from the need for a nonzero pulse-height bias to discriminate against noise. Sometimes a rather high bias improves the signal-to-background ratio. This selection of events with a pulse height above a chosen bias introduces problems because of the different types of neutron interactions in the scintillator[23]). And it is not a straightforward procedure to find out which interactions result in a pulse-height above the bias and which do not. The position of the bias within the pulse-height spectrum must be accurately located.

Above about 12 MeV the reaction $^{12}C(n,n')3\alpha$ which has a threshold at 8.3 MeV contributes about one half of the total nonelastic cross section[19]), and therefore it must not be neglected. However, the kinematics of this reaction are not well known, so there is little information on the division of the reaction energy among the reaction products. Because of the nonlinearity of the light-response curve, it does not help much to know the total dissipated energy.

Because of these difficulties, several[6,15–18]), but not

* Work performed under the auspices of the U.S. Atomic Energy Commission.

† On leave from the University of Vienna, Vienna, Austria.

TABLE 1

Efficiency and light-response data of organic scintillators in the literature. (The last number in "Dimensions" gives the sensitive length; "Method" is explained in sec. 2.)

Dimensions (cm)	EFFICIENCY *E*-range (MeV)	EFFICIENCY Bias (MeV E_p)	EFFICIENCY Method	RESPONSE FUNCTION Particle	RESPONSE FUNCTION *E*-range (MeV)	Ref.
Anthracene						
3.8 × 1.9				p	< 15	25, 43
Stilbene						
1 × 0.5				p	1.5 ... 10	44
& 2 × 1						
small			calculated	p(α)	1 ... 25	45
various	0.5 ... 18	various	calculated			16
2.5 × 1.3				p	< 15	25, 43
5.1 × 5.1				p	< 14	46
PILOT(B)						
5.1 × 3.8	< 5	low	comparison			26
5 × 5	1 ... 14	0.5 & 3.5	n–p, calc.			17
1.2 × 1	13.9, 15.6	various	ass. particle			32
3.4 × 2	< 1.5	very low	comparison	p	< 1.5	27
5.1 × 5.1	0.2 ... 3	0.19	n–p, calc.			36
5.1 × 5.1				p	< 15	25, 43
5.1 × 5.1				p	< 14	46
12.7 × 3.8	0.4 ... 2.5	low	d–D, p–T, n–p, calc.			35
NE 102						
5.1 × 1.3				p	3 ... 14	47
7.6 × 17.8				p, d(t, α)	28 ... 147.5	48
3.8 × 2.5				p	0.14 ... 2.3	49
17.6 × 10	21, 25, 29	≈ 6	ass. particle, calculated			7
× 2.5	< 6.5	≲ 0.4	n–p, comp.	p	< 2.5	37
4.4 × 5.1				C	< 5	50
12.7 × 30.5	13 ... 70(... 170)	1, 2, 4(16)	ass. particle			8, 9
5.1 × 5.7				p	< 15	25, 43
5 × 8	< 5	0.6	calculated			51
10.3 × 5.1	5 ... 40	3 & higher	differential			10
12.7 × 2.5	0.3 ... 8.5	low	d–D, p–T, n–p, calc.			35
NE 102A						
12.7 × 5.1	0.07 ... 6.0	very low	comparison			28
10.2 × 2.5	< 2	low	n–p, comp.			29
& × 5.1						
5 × 8	< 5	0.6	calculated			51
30 × 28.6	20 ... 130	6	comparison			11
NE 211						
12.7 × 12.7	< 14	low				21, 52
4.7 × 4.6	0.2 ... 21.8	various	calculated	p, α, C	0.1 ... 40	53

NE 213						
5.1 × 6.4	0.3 ... 3.5	0.2	comp., calc.	p, (α, C)	0.7 ... 14	18
& 7.6 × 10.2						
No data				p	< 5	37
5.1 × 5.1	0.2 ... 14.4	various	calculated	p, α, C	< 20	21
3.8 × 3.8				α	4.8, 6.1	54
3.2 × 3.8				C	< 5	50
5 × 5	0.1 ... 20	various	calculated	p, α, C	0.1 ... 20	20
12.7 × 12.7	< 14	various	calculated			21, 52
5.1 × 6.4	< 20	low	comparison	p	< 20	6
5.1 × 5.7				p	< 15	25, 43
4.7 × 4.6	0.2 ... 21.8	various	calculated	p, α, C	0.1 ... 40	53, 55
12 × 2.6	2.7, 14.5	various	ass. particle			30
& 12 × 6.1						
5.1 × 5.1	1 ... 9					56
5.1 × 5.1				p	< 14	46
4 × 10	0.6 ... 3.2	0.65	n–p, calc.			38
12.7 × 3.8	0.3 ... 9	low, various	d–D, p–T, n–p, calc.			35
NE 214						
4.2 × 5				p	< 15	57
NE 218						
12.7 × 7.6	< 5	low	ass. part., n–p			31
5.1 × 5.1				p	< 14	46
2.5 × 2.5				p	1.4 ... 30	58
NE 224						
× 6.4	< 7	0.4	n–p, calc.	p	< 3	37
7.6 × 15.2 × 30.5	4 ... 36	not given	ass. particle			33
7 × 45	20 ... 340	high	ass. particle			12
NE 228						
11.1 × 4.4	5 ... 40	3	differential			10
NE 230						
4.4 × 5.1				p	< 15	25, 43
Other plastic						
20 × 20 × 15 &	4 ... 76	4	ass. particle			13
20 × 60 × 15						
9 × 10.2	3 ... 250	2.3	calculated			22
× 82	1.7, 2.1, 3.0 GeV/*c*	high	ass. particle			59
Other liquid						
× 5.1	2 ... 3.5		d–D			34
2.5 × 1.9	15 ... 120	1.7	differential			14
3 × 3				α	0.8 ... 8	41
spheres:	< 14	0.6/1.5	ass. part., calc.	p	< 16	60
4.7, 10.7						
100 × 108 × 36	70 ... 390	25, 48	ass. part., calc.			61
122 × 30.5 × 15.2	50 ... 300	5 ... 30	ass. part., calc.			62

all[19,22,23]), codes for the efficiency calculation neglect the n–3α process in carbon.

Even if all reactions are taken into account, an adjustment of the calculation to experimental data is necessary. This becomes necessary not only because of the lack of information on the reaction mechanisms (and uncertainties in the cross sections) but also because of uncertainties in the response curves of the detector for the various particles. These curves differ for different types of scintillators, but even for scintillators of the same type there may be a noticeable difference[24]). This is due to differences in impurities, in the light attenuation[25]) and in the pulse-shaping time constants which affect the pulse-height contributions with different decay times differently. Therefore it seems necessary to check an efficiency calculation at several energies by an experiment, if a precision of better than about 5% is necessary.

Several methods have been applied to determine the efficiency experimentally.

1) Point-by-point comparison with a calibrated detector (long counter, counter telescope, fission chamber, etc.)[6,11,18,26–29]).

2) Associated particle method. The flux of neutrons impinging on the detector is measured by detecting the associated charged particles of the neutron-producing reaction[30–32]). At high energies the associated recoiling protons of the elastic n–^{1}H scattering are detected[7–9, 12,13,33]).

3) The differential method[10,14]) as introduced by Bowen et al.[14]). If the carbon-to-hydrogen ratio of two hydrocarbon scintillators differs, then the absolute efficiency of either can be calculated from a measurement of their efficiency ratio with the knowledge of the neutron total cross sections of hydrogen and carbon.

4) Comparison of the yields of an angular distribution measurement with the corresponding differential cross sections, ^{2}H(d,n)^{3}He [34]), ^{3}H(p,n)^{3}He [35]), or ^{1}H(n,n)^{1}H [17,29,31,36–38]).

With the last method, one can obtain only a relative efficiency curve. If necessary, the absolute scale can be established by measuring the incoming flux (either with a calibrated detector or by the associated particle method) or by normalizing the curve (by means of one absolute measurement or a calculation).

3. Method

In order to minimize some of the systematic errors, it is advisable to measure the detector efficiency in the same geometrical arrangements (same flight path for equal acceptance angle of the detector and for equal attenuation by the air, same collimator and shielding configuration) and at counting rates similar to those in the main experiment. Therefore, if the detector is to be used in a scattering experiment, elastic scattering from hydrogen is the best choice.

The absolute efficiency, ε_{abs}, as derived from an angular distribution measurement for incoming neutrons with an energy E_0 is given by

$$\varepsilon_{abs}(E, B) = \varepsilon_{abs}(E_0, \theta_L, B) = h \cdot Y_H/[N_{Mon} \cdot \sigma_H(E_0, \theta_L)], \quad (1)$$

TABLE 2

Experimental conditions for the individual angular distributions.

Set no.	Neutron production E_0 (MeV)	ΔE_0 (fwhm) (MeV)	Reaction type	Scatterer Distance from target (cm)	Φ	Mass of CH_2 sample (g)	Settings No. of biases	No. of angles
1	3.7	0.14	T(p,n)^{3}He	12	45°	2.82	11	7
2	6.9	0.20	D(d,n)^{3}He	20	55°	2.82	6	5
3	8.5	0.10	T(p,n)^{3}He	12	45°	2.82	11	7
4	12.5	0.09	T(p,n)^{3}He	20	45°	11.31	11	4
5	13.6	0.09	T(p,n)^{3}He	12.5	70°	7.48	2	4
6	22.4	0.24	T(d,n)^{4}He	20	30°	11.31	1	11
7	23.7	0.15	T(d,n)^{4}He	12	45°	11.31	11	3
8	25.0	0.15	T(d,n)^{4}He	20	45°	11.31	10	13
9	27.1	0.13	T(d,n)^{4}He	12	45°	11.31	11	4
10	27.1	0.12	T(d,n)^{4}He	20	20°	11.31	1	8
11	28.5	0.12	T(d,n)^{4}He	20	45°	11.31	10	5
12	30.0	0.13	T(d,n)^{4}He	12.5	70°	7.48	1	4

with

E = scattered neutron energy,
B = pulse-height discriminator bias,
θ_L = scattering angle (in the laboratory),
h = proportionality factor,
Y_H = number of counts in the hydrogen peak of the time-of-flight spectrum, corrected for attenuation and dead time,
σ_H = differential cross section for neutron scattering in the laboratory system, and
N_{Mon} = normalization number, proportional to neutron dose accepted by the scattering sample.

The proportionality factor, h, drops out if one is interested only in the relative efficiency, $\varepsilon(E,B)$, as is the case in angular distribution measurements that are being normalized by means of cross section standards. h contains the proportionality factor between N_{Mon} and the actual neutron dose, the solid angle suspended by the neutron detector with respect to the source, and the actual number of scattering hydrogen nuclei. The use of the differential $^1H(n,n)^1H$ cross section as a standard is discussed by Hopkins and Breit[39]).

4. Experimental details

The angular distributions of monoenergetic neutrons scattered from hydrogen in a polyethylene (CH_2) sample were measured by the time-of-flight (TOF) method. The neutron-producing reactions used and the incoming energies, E_0, are listed in table 2 together with other experimental conditions.

4.1. The primary neutron beam

The bunched beam of a Van-de-Graaff accelerator with a typical burst length of 1 ns was used for neutron production. The $\approx$ 3 cm long neutron target[40]) was filled with tritium (or deuterium) gas at a typical pressure of 2.8 bar (41 psia). For a proton beam, the entrance foil was 9.57 mg/cm^2 of ^{58}Ni and the beam stop was made of ^{58}Ni; for a deuteron beam the foil was 7.92 mg/cm^2 molybdenum and the beam stop was made of gold.

The normalization number N_{Mon} of eq. (1) was obtained in two independent ways. A monitor detector viewed the target under an angle of 110°. This position allowed enough space around the neutron target for the experimental setup. The monitor detector had a thin plastic scintillator and utilized the TOF method (flight path about 1.27 m) for isolation of the neutron peak of interest. The counts in the time window of interest, N_{Mon}, are proportional to the number of neutrons produced and since the acceptance angle of the scattering sample stays the same throughout the experiment, it is proportional to the number of neutrons impinging on the sample.

If the number of target nuclei (respectively the areal density) in the neutron-producing target stays constant[40]), the integrated beam current hitting this target is proportional to the dose. Therefore the beam current integrator was used to cross-check the monitor detector.

4.2. The scattering sample

Perhaps the greatest deficiency of using hydrogen as a cross-section standard is that it is not available as a solid sample in the pure state. Either it must be contained, or a solid hydrogen compound must be used. One of the best choices is polyethylene. It has a high hydrogen concentration, it is readily available, and the neutron cross sections of carbon, its only other constituent, are rather well known. To correct for the background at the position of the hydrogen peak, a separate run with a graphite scatterer is necessary to determine the background stemming from the carbon.

There is another advantage (besides the small uncertainty of the cross sections) in using hydrogen for the efficiency measurement. Because of its small mass, rather large energy ranges can be covered in angular distribution measurements at each incoming energy. Even with the restriction to an angle range between 20° (because of shielding problems of the primary neutron source at smaller angles) and about 50° (large energy spread at bigger angles due to kinematics), a factor of 2 between minimum and maximum energy for the efficiency measurement is obtained.

The restriction to a small angular range (35° $\pm$ 15°) allows us to take advantage of the flat plate geometry. Compared to the geometry using cylindrical samples, this offers two advantages:

- for the same mass, the multiple scattering probability is smaller;

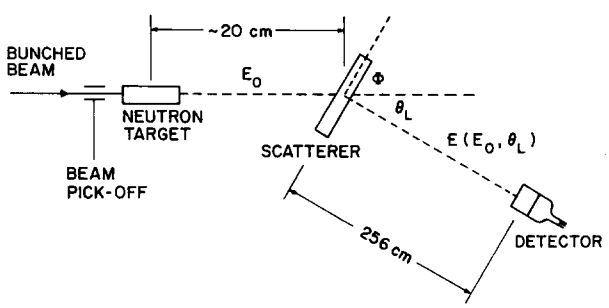

Fig. 1. Geometry for the elastic neutron scattering from a flat CH_2 plate.

– the attenuation correction can be calculated in a straightforward way.

The scattering samples, rectangular slabs with lateral dimensions of about 4 cm by 3 cm, were located at 0° with respect to the charged-particle beam (see fig. 1). The sample thickness (0.25 cm to 1.00 cm for CH_2) was chosen so that the attenuation in the slab was less than 10% in nearly all cases. For thin flat CH_2 samples, the attenuation correction, a_{CH_2}, can be obtained from

$$a_{CH_2} = \exp\{t[n_C\sigma_C(E_0) + n_H\sigma_H(E_0)]/2\sin\Phi + \\ + t[n_C\sigma_{C_n}(E) + n_H\sigma_H(E)]/2\sin(\Phi+\theta_L)\}, \quad (2)$$

t = sample thickness,
n_C = number of carbon atoms per volume,
σ_C = total cross section of carbon,
n_H = number of hydrogen atoms per volume,
σ_H = total cross section of hydrogen,
Φ = angle of scatterer with respect to beam,
σ_{C_n} = total nonelastic cross section of carbon.

The first part of the exponent takes the attenuation of the ingoing beam into account, the second part that of the outgoing beam (multiple scattering). The multiple-scattering correction works under the assumption that no event is recorded in the time window of interest, if the second event was a nonelastic scattering from carbon or an elastic one from hydrogen, both degrading the neutron energy appreciably. Elastic in- and out-scattering from carbon is assumed to cancel. These crude assumptions are justified by abundant experimental evidence that eq. (2) gives agreement in the yields to better than 1% even for slabs about twice as thick as the ones actually used.

To correct properly for the background, each hydrogen yield, Y_H, had to be derived from three individual runs: one foreground run (with CH_2) and two background runs, one using a graphite sample C of similar geometrical dimensions and one using no sample at all (indicated by the index MT).

Then Y_H can be determined from the following expression:

$$Y_H = a_1 Y_{CH_2} - k_2 \cdot a_2 Y_C - (a_1 - k_2 a_2) Y_{MT}, \quad (3)$$

a_i = attenuation correction for the sample,
Y_i = measured individual yields in the time window of interest,
k_2 = ratio of C atoms in the CH_2 sample and the C sample.

The individual yields, Y_i, are obtained from the TOF spectra by adding up the counts in that time interval in which neutrons scattered from H arrive. Besides, all runs must be normalized to a standard number of monitor counts, N_{Mon}, and the dead time correction must be applied. The latter was done by counting the number of bursts after each recorded event during which the electronics could not process other events. Division by the number of all bursts gives the percentage-dead-time if the beam current is reasonably constant and low enough so that multiple events per burst can be neglected.

At intermediate energies (around $E_0 = 10$ MeV) the peak of neutrons inelastically scattered from carbon (exciting the 4.4 MeV level) frequently coincides with the hydrogen peak. Then $k_2 a_2$ in eq. (3) is not necessarily the proper adjustment factor, because the attenuation of these neutrons is different in the CH_2 sample and in the C sample. The effect of extremely different adjustments on Y_H was never more than 2%. Therefore, in these cases an adjustment error of $\pm 1\%$ takes care of this uncertainty.

At energies above about 20 MeV the hydrogen peak overlaps with the background peak (consisting of the primary neutron peak, and of the elastic and inelastic carbon peaks). The carbon peaks are attenuated differently in the polyethylene and in the graphite sample, introducing an error when using eq. (3) for background subtraction. This error increases with increasing overlap of the peaks, limiting the useful energy range of the simple method described here to below about 25 MeV. At 25 MeV background subtraction errors up to 5% can be expected unless the background is adjusted in a more realistic way than that implied by eq. (3).

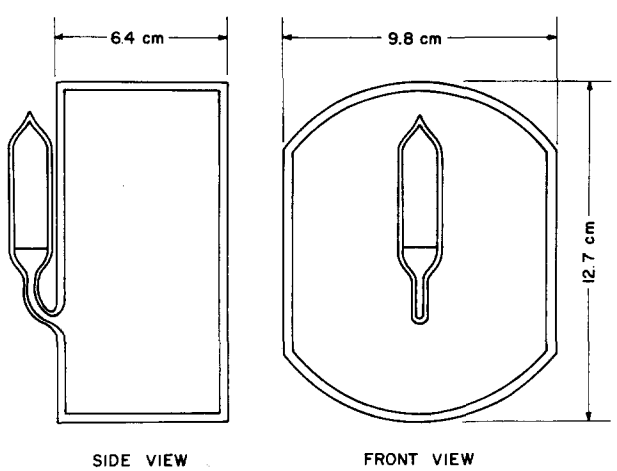

Fig. 2. Side and front view of the glass container for the liquid scintillator.

The scattering samples were mounted on a sample wheel and changed by remote control.

4.3. The detector

The shape of the glass housing for the liquid scintillator is shown in fig. 2. The small secondary container connected to the main container by a thin tube accepts the gas bubbles of the scintillator liquid. All bubbles must be removed from the main container because they have a detrimental effect on the light collection. The side with the secondary container views the scatterer. The opposite, flat side is optically coupled to a 5 in. 56AVP photomultiplier. The sensitive length of the scintillator is about 5.7 cm. There is a light-tight housing around the detector with an entrance window of 0.26 cm aluminium.

The glass housing was sent to Nuclear Enterprises, Winnepeg, Canada, to be filled with NE218, which has an especially high hydrogen concentration. However, the results of this investigation are inconsistent with such high H concentration. Consequently, a Raman spectroscopy comparison with a NE213 and a NE218 sample was made by L.H. Jones of Group CNC-4 of this Laboratory, showing the similarity of the Raman spectrum of our detector with that of the NE213 sample rather than with that of the NE218 sample. Therefore one must assume that the glass container had been filled erroneously with NE213. This mistake is, however, of no importance for the results of previous measurements done with this detector (claimed to be NE218 as reported, e.g., in ref. 1) because in all cases the actual efficiency had been measured, not calculated.

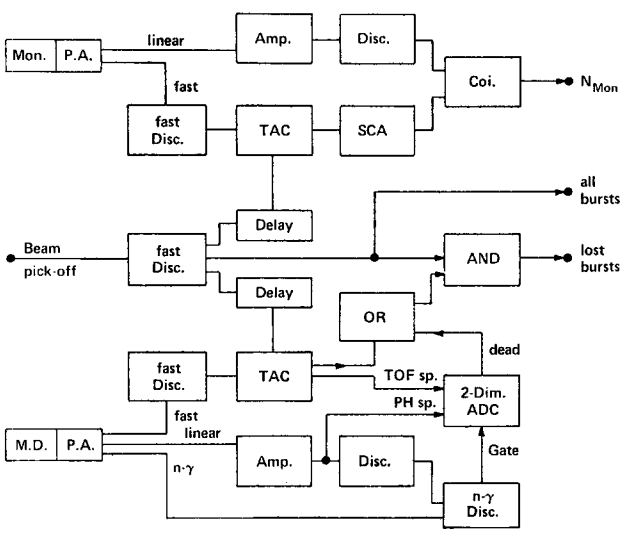

Fig. 3. Simplified circuit diagram. Mon. = monitor detector, P.A. = preamplifier, Amp. = amplifier, Disc. = discriminator, Coi. = (slow) coincidence, TAC = time-to-amplitude converter, SCA = single channel analyzer, M.D. = main detector.

The efficiency was measured under the same conditions that occur in the actual angular distribution measurements for which the detector is mainly used. Thus systematic errors such as attenuation by the air and inscattering from the collimator and the shielding material are minimized. The large shield consisting of copper, lead, and polyethylene with a copper collimator and a tungsten shadow bar could be moved around the center of the scattering sample with the help of air pallets. The scattering angle was measured by means of a digitizer and was known to within $\pm 0.1°$.

4.4. The electronics

A simplified schematic of the electronic setup is given in fig. 3. There are two independent TOF branches, one for the monitor and one for the main detector (M.D.). The start pulses for the time-to-amplitude converter (TAC) are derived from the fast signals of the photomultiplier, the stop pulses from signals of the beam pickoff.

In the monitor branch, the neutron peak in the TOF spectrum was selected by means of a single-channel analyzer (SCA) giving the number N_{Mon} for the normalization of the individual runs.

From the main detector three signals were derived:

- the fast signal for the start of the TAC,
- the linear (slow) signal for the pulse-height spectrum,
- the n–γ signal for the n–γ discriminator.

The TOF spectrum and the linear spectrum were fed into two ADC's (256 channels) connected on-line to an SDS-930 computer, giving two-dimensional information on energy (TOF) and pulse-height. The gating signals for the ADC's were the output pulses of the n–γ discriminator. The dead time was measured by means of an OR-gate and an AND-gate as shown in fig. 3, using the method described in section 4.2.

4.5. Pulse-height calibration

The light output from organic scintillators in response to electrons is sufficiently proportional to the energy so that the pulse-height is commonly expressed in electron energy. The most convenient way to introduce electrons into the scintillator is by generation of Compton electrons by γ-rays. The pulse-height at half the height of the Compton peak does not really correspond to the energy of the Compton edge, but is higher by a factor of 1.04 ± 0.01[41]) or 1.05 ± 0.01[6]). The

response curve, the ratio between pulses from protons and from electrons of the same energy, was obtained by comparing the pulse-height spectra for mono-energetic neutrons with the Compton edge of ^{137}Cs which corresponds to 478 keV electron energy. From this the equivalent proton energies of the pulse-height discrimination biases, set at multiples of one "Cs-unit", were derived (see table 3).

TABLE 3

Pulse-height-to-energy conversion and parameters for calculated fits. (Constant parameters for the fit: $B' = 0.44B^*$, $n_H \cdot t = 0.26 \times 10^{24}$ at/cm^2.)

Pulse-height bias (Cs units)	Corresponding proton energy (MeV)	B^* (MeV)	k
0.4	1.1	1.06	1.026
0.5	1.3	1.21	1.021
1.0	2.0	1.94	0.971
1.5	2.6	2.53	0.945
2.0	3.2	3.05	0.927
2.5	3.7	3.59	0.911
3.0	4.2	4.08	0.899
3.5	4.7	4.53	0.891
4.0	5.1	4.95	0.885
4.5	5.5	5.40	0.882
5.0	5.9	5.80	0.874

The conversion in table 3 is subject to an error of about 5%. As this error does not enter into the measurement of the efficiency but only into a calculation, no attempt was made to reduce it. For the measurement it is important only that the pulse-height discrimination bias can be set reproducibly.

5. Data reduction and results

As pointed out in section 4.4, the TOF and the pulse-height of each event were recorded simultaneously. The on-line computer stored up to 11 TOF spectra, selecting the events according to the pulse-height biases. Dead-time corrections and normalizations to the same number, N_{Mon}, of monitor counts were done on-line.

The tape generated by the on-line computer was then evaluated off-line. The differential TOF spectra of each run were summed to give the integral spectrum above the bias of interest. The yield for the hydrogen peak was then calculated by subtracting the two background contributions from the total counts [according to eq. (3)] after proper normalizations. Thus, yields, Y_H, for each of the 12 angular distribution measurements listed in table 2 were derived. Each distribution gave the energy dependence of the detector efficiency for several energies, but as h in eq. (1) differs for each distribution, the results have different scale factors. Having many overlapping energies at hand, one arrives at an interleaving system of proportionality factors and one can join the results from the different sets reliably.

The final scale was obtained by calculating the absolute efficiency at one energy in a simplified way and by normalizing all points to this calculated value. To decrease the influence of multiple scattering, this energy should be as high as possible with respect to the bias. On the other hand, it must be low enough that nonelastic reactions in carbon do not show up. The shape of the curves suggests that 12 MeV with a $1 \times$ Cs bias is a good choice.

The simplifications of the calculation consist of the following assumptions:

1) Only scattering from hydrogen is important.
2) The effective areal density for the second scattering is $t \cdot n_H/2$. (This is a good approximation if the bias B is much smaller than E. Then all first scatters resulting in a pulse-height below B – the only ones that increase the efficiency in the case of a second scatter – are small angle scatters which do not change the flight direction much.)
3) The effective neutron energy after the first scattering is $E - B/2$.
4) On the average all pulses above $B/2$ in the second scattering process will result in a pileup pulse above B.

Neglecting the multiple-scattering contribution of carbon will make the calculated value lower than the actual one. The opposite is true for the neglect of the flux attenuation by the carbon. Making the above 4 simplifications causes at most an error of $\pm 10\%$ at the chosen energy of 12 MeV.

Thus we arrive at the formula

$$\varepsilon_{abs}(E, B) = \frac{E-B}{E}\left[1-e^{-t\cdot n_H \sigma_H(E)}\right] \times \times \left\{1 + \frac{B}{E-B/2}\left[1-e^{-\frac{1}{2}t\cdot n_H \sigma_H(E-B/2)}\right]\right\}. \quad (4)$$

For $E = 12$ MeV, $B = 2.0$ MeV, and $t \cdot n_H = 0.27 \times 10^{24}$ at/cm^2, one obtains

$$\varepsilon_{abs}(12\,\text{MeV}, 1 \times \text{Cs}) = 16.5\%.$$

This number was used for the final normalization of the efficiency points. It agrees within the assumed

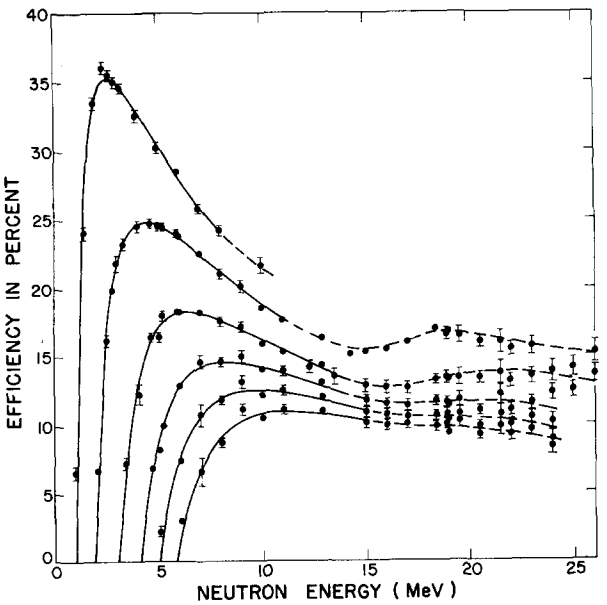

Fig. 4. Measured efficiency points for biases at 0.4, 1.0, 2.0, 3.0, 4.0 and 5.0 times Cs and calculated fits (solid lines). The dashed lines are handfitted.

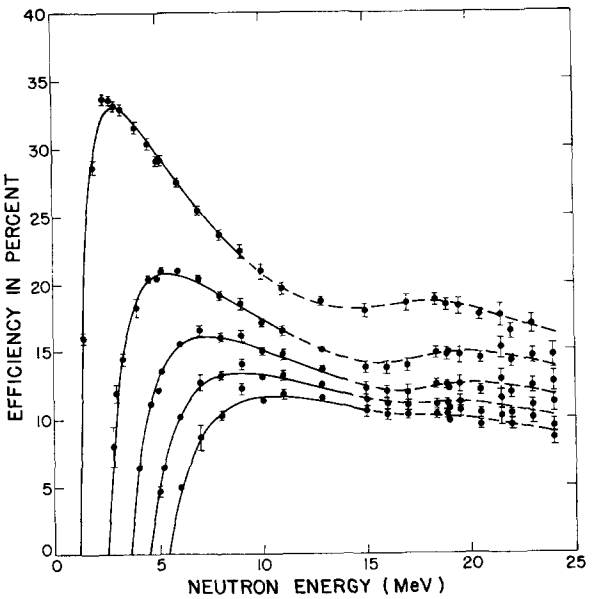

Fig. 5. Same as fig. 4, but for biases at 0.5, 1.5, 2.5, 3.5, and 4.5 times Cs.

errors with a counter telescope comparison that gave

$$\varepsilon_{\mathrm{abs}}(12\,\mathrm{MeV},\ 1 \times \mathrm{Cs}) = (15.8 \pm 0.8)\,\%\,.$$

The measured values for 11 biases are shown in figs. 4 and 5, together with their statistical errors. In addition, there are error contributions from the following sources:

1) uncertainty in the $^1\mathrm{H(n,n)^1H}$ differential cross section,
2) energy uncertainty and energy spread,
3) errors in the correction for attenuation and multiple scattering,
4) changes in the pulse-height bias,
5) errors in the background subtraction,
6) errors in N_{Mon}, the normalization within each angular distribution,
7) errors in joining individual sets.

Most of these errors are reduced by measuring neutrons of the same energy under different conditions (different incoming energy and scattering angle). Besides, a smooth curve through the data points further reduces random errors. But, especially the joining error could result in a systematic error tilting the efficiency curve. This tilt would show up even in a calculated fit. For energies below 12 MeV the tilt is estimated to be less than $\pm 1.5\%$ per 10 MeV, for energies below 22 MeV less than $\pm 2.5\%$ per 10 MeV.

6. Calculations and discussion

Before one derives an analytical expression to fit the data one must justify the assumption that the efficiency curve is smooth. This is not obvious, because the total carbon cross section, which has many narrow resonances, is comparable to that of hydrogen and the numbers of these two kinds of nuclei in the scintillator are comparable as well.

In thin scintillators where multiple scattering is negligible, the elastic interaction with carbon produces pulses well below the pulse-height biases used in this experiment. In thick detectors, multiple elastic scattering from carbon alone still does not produce pulses above the bias.

Hydrogen–carbon events increase the efficiency only if the first event produces a pulse just below the bias and the pileup of the carbon event makes it bigger than the bias. This is generally a very small contribution, and any structure in it would not show up.

In a carbon–hydrogen event the first collision degrades the neutron energy only slightly (maximum energy loss 28%) so that the situation is about the same as without a first collision except for the pileup with the small carbon pulse and a somewhat different neutron path through the detector.

Nonelastic carbon interactions are of little importance as long as the secondary particles do not contribute to pulses above the bias. If the neutron energy

is high enough, all carbon breakups will give pulses above the bias and the structure of this cross section will show up in the shape of the efficiency curve. But with the biases in question this would only affect energies above about 12 MeV where the nonelastic cross section does not show a pronounced structure.

In addition, the energy spread of the incoming neutrons and the kinematic spread of the scattered neutrons would tend to wash out narrow structures.

As the shape due to nonelastic interactions reflects the cross section for these processes, there is practically no chance of fitting this part of the efficiency curve by a simple analytical expression. Therefore an attempt was made only to fit that part of the efficiency curves where elastic scattering from hydrogen is dominant[42]).

Of course, it is desirable to find an expression that uses only physically meaningful parameters. These parameters are: σ_H, n_H, t, E, B and k, k being a scale-adjustment factor necessary because the measured points have been normalized with a scale uncertainty of about $\pm 10\%$ (see sec. 5).

All these factors are straightforward. But with them alone no reasonable fits can be expected because of two effects which are illustrated in fig. 6. This figure shows the (simplified) pulse-height spectrum of recoil protons for monoenergetic neutrons of energy E without multiple scattering. Using a nonlinear scale for the pulse height (e.g., equivalent proton energy units) simplifies the picture. The first effect, for which one must correct, is the pulse-height resolution of the scintillation counter. This changes the rectangular distribution (dashed) to the smeared-out distribution (solid line). Assume, for instance, that the bias coincides exactly with E. Then no events would be counted having the ideal distribution, but there are counts in the real case above the bias. For the ideal distribution a bias at B^* would give the same number of counts as a bias at E in the real case. This equivalent bias B^* differs the more from the ideal bias, the higher it is with respect to E. Therefore no reasonable calculated fit can be expected through the low-energy points of the efficiency curve assuming an ideal (rectangular) pulse-height distribution and a constant bias, essential for a simple calculation. Excluding these lowest-energy points one can expect a good fit with a constant bias, B^*, which is close to the ideal bias B (see table 3).

The second effect we must consider is the efficiency increase from multiple scattering. If only double elastic scattering from hydrogen were important, a formula similar to eq. (4) would do the job. However, the average path and therefore the effective areal density of hydrogen for the second scattering process would increase with smaller E/B ratios, thus increasing the multiple scattering contribution for smaller energies. This increase can be simulated by a virtual bias $B_{virt} = B - B'$ below the actual bias B (see fig. 6). Further, one must shift E by the same amount, so that for $E = B$ the efficiency becomes zero.

These two conditions lead to the following expression.

$$\varepsilon(E, B) = k\left(1 - \frac{B^* - B'}{E - B'}\right)[1 - e^{-t \cdot n_H \sigma_H(E)}]. \quad (5)$$

Best fits for all 11 curves were obtained with $B^* \approx B$ and $B' = 0.44\, B^*$. It is pleasing that B' is a constant fraction of B^*. The only unconstrained adjustment factor is k. This factor is listed in table 3 together with the B^* values. Its energy dependence is shown in fig. 7. If eq. (5) described the processes correctly, k would be a constant close to 1.0, independent of energy. The strong increase in k for small biases

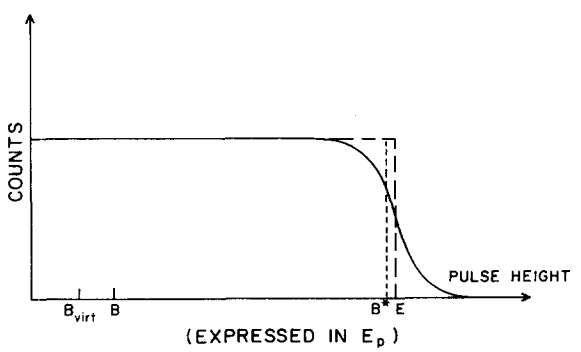

Fig. 6. Idealized pulse-height distribution of recoil protons for monoenergetic neutrons (see text).

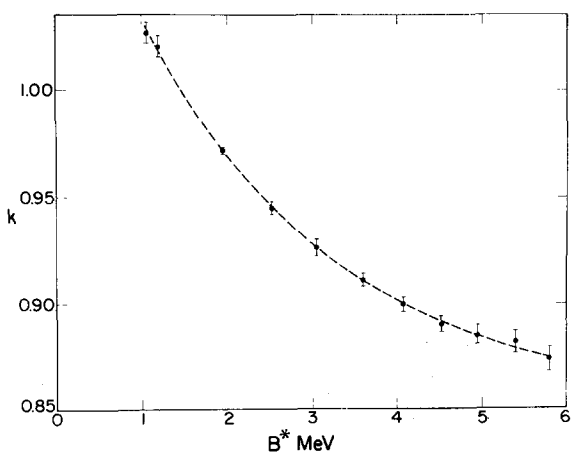

Fig. 7. Energy dependence of the adjustment factor, k, of the calculated fit.

indicates that the approximations leading to eq. (5) are less meaningful for low biases. This was to be expected from the neglect of the carbon contributions, which have greater effect at lower biases.

Part of the data was taken for the $^4He(n,n)^4He$ experiment[1]) with the help of J. C. Hopkins, A. Niiler, J. D. Seagrave and J. T. Martin. R. Lucke helped with the data reduction. I am thankful to these people and to the staff of the Van de Graaff for their assistance.

References

1) A. Niiler, M. Drosg, J. C. Hopkins, J. D. Seagrave and E. C. Kerr, Phys. Rev. C4 (1971) 36.
2) J. B. Birks, *The theory and practice of scintillation counting* (Pergamon Press, Oxford, 1964).
3) W. D. Allen, *Neutron detection* (Newnes, London, 1960).
4) R. B. Owen, IRE Trans. Nucl. Sci. NS-9, no. 3 (1962) 285.
5) W. B. Reid and R. H. Hummel, Can. Nucl. Tech. **5**, no. 1 (1966) 36.
6) A. A. O'Dell, C. W. Sandifer and R. B. Knowlen, Neutron counting efficiency and charged particle response of an NE-213 fluor detector, EGG (1968) 1183.
7) G. Gatti, P. Hillman, W. C. Middelkoop, T. Yamagata and E. Zavattini, Nucl. Instr. and Meth. **29** (1964) 77.
8) F. P. Brady, J. A. Jungerman, J. C. Young, J. L. Romero and P. J. Symonds, Nucl. Instr. and Meth. **58** (1968) 57.
9) J. C. Young, J. L. Romero, F. P. Brady and J. R. Morales, Nucl. Instr. and Meth. **68** (1969) 333.
10) J. B. Hunt, C. A. Baker, C. J. Batty, P. Ford, E. Friedman and L. E. Williams, Nucl. Instr. and Meth. **85** (1970) 269.
11) D. G. Crabb, J. G. McEwen, E. G. Auld and A. Langsford, Nucl. Instr. and Meth. **48** (1967) 87.
12) A. S. L. Parsons, P. Truoel, P. A. Berardo, R. P. Haddock, L. Verhey and M. E. Zeller, Nucl. Instr. and Meth. **79** (1970) 43.
13) C. E. Wiegand, T. Elioff, W. B. Johnson, L. B. Auerbach, J. Lach and T. Ypsilantis, Rev. Sci. Instr. **33** (1962) 526.
14) P. H. Bowen, G. C. Cox, G. B. Huxtable, A. Langsford, J. P. Scanlon, G. H. Stafford and J. J. Thresher, Nucl. Instr. and Meth. **17** (1962) 117.
15) V. G. Zolotukhin, G. G. Doroshenko and B. A. Efimenko, Atom. Energ. **15** (1963) 194.
16) V. G. Zolotukhin and G. G. Doroshenko, Atom. Energ. **18** (1965) 287.
17) H. Grässler and K. Tesch, Nucl. Instr. and Meth. **10** (1961) 353.
18) R. Batchelor, W. B. Gilboy, J. B. Parker and J. H. Towle, Nucl. Instr. and Meth. **13** (1961) 70.
19) R. J. Schuttler, Efficiency of organic scintillators for fast neutrons, ORNL-3888 (1966).
20) V. V. Verbinski, W. R. Burrus, R. M. Freestone and R. Textor, Proton-recoil neutron spectrometry with organic scintillators, Proc. IAEA Symp. *Neutron monitoring for radiological protection* (Vienna, 1966); ORNL-P-2471.
21) V. V. Verbinski, J. C. Courtney, W. R. Burrus and T. A. Love, The response of some organic scintillators to fast neutrons, ORNL-P-993 (1965).
22) R. J. Kurz, A 709/7090 FORTRAN II program to compute the neutron-detection efficiency of plastic scintillator for neutron energies from 1 to 300 MeV, UCRL-11339 (1964).
23) R. E. Textor and V. V. Verbinski, 05S: A Monte Carlo code for calculating pulse height distributions due to monoenergetic neutrons incident on organic scintillators, ORNL-4160 (1968).
24) R. L. Craun and D. L. Smith, Nucl. Instr. and Meth. **80** (1970) 239.
25) P. Kuijper, C. J. Tiesinga and C. C. Jonker, Nucl. Instr. and Meth. **42** (1966) 56.
26) L. Cranberg and J. S. Levin, Phys. Rev. **103** (1956) 343.
27) L. E. Beghian, S. Wilensky and W. R. Burrus, Nucl. Instr. and Meth. **35** (1965) 34.
28) H. Condé, G. During and J. Hansén, Ark. Fys. **29** (1965) 307.
29) J. M. Adams, E. Barnard, A. T. G. Ferguson, W. R. McMurray and I. J. Van Heerden, Nucl. Instr. and Meth. **34** (1968) 21.
30) T. A. Love, R. W. Peelle, R. T. Santoro, N. W. Hill and R. J. Schuttler, Measurement of the absolute efficiency of NE-213 organic phosphors for the detection of 14.4 and 2.6 MeV neutrons, ORNL-3714, vol. II; ORNL-3893 (1966); T. A. Love, R. T. Santoro, R. W. Peelle and N. W. Hill, Rev. Sci. Instr. **39** (1968) 541.
31) W. R. Jackson, A. S. Divatia, B. E. Bonner, C. Joseph, S. T. Emerson, Y. S. Chen, M. C. Taylor, W. D. Simpson, V. Valkovic, E. B. Paul and G. C. Phillips, Nucl. Instr. and Meth. **55** (1967) 349.
32) O. Meyer, Absoluteichung von Neutronendetektoren bei Neutronenenergien von 13.9 und 15.6 MeV, IKF-6 (1962).
33) P. Berardo, R. P. Haddock and M. Zeller, Liquid scintillator detection efficiency for 4 to 36 MeV neutrons, UCLA-34P106-1 (1967).
34) J. E. Hardy, Rev. Sci. Instr. **29** (1958) 705.
35) S. T. Thornton and J. R. Smith, to be published.
36) R. Honecker and H. Grässler, Nucl. Instr. and Meth. **46** (1967) 282.
37) J. B. Czirr, D. R. Nygren and C. D. Zafiratos, Nucl. Instr. and Meth. **31** (1964) 226.
38) K. Wiesner, K. Trützschler, D. Schubert and R. Neumann, Nucl. Instr. and Meth. **78** (1970) 131.
39) J. C. Hopkins and G. Breit, Nucl. Data Tables A9 (1971) 137.
40) D. K. McDaniels, I. Bergqvist, D. Drake and J. T. Martin, Nucl. Instr. and Meth. **99** (1972) 77.
41) K. F. Flynn, L. E. Glendenin, E. P. Steinberg and P. M. Wright, Nucl. Instr. and Meth. **27** (1964) 13.
42) R. M. Freestone, Jr., DORO 2: An organic scintillator pulse height analysis code, ORNL-TM-2112 (1968).
43) D. L. Smith, R. G. Polk and T. G. Miller, Nucl. Instr. and Meth. **64** (1968) 157.
44) H. W. Broek and C. E. Anderson, Rev. Sci. Instr. **31** (1960) 1063.
45) A. Huck and G. Walter, Nucl. Instr. and Meth. **59** (1968) 157.
46) B. A. Pohl, J. D. Anderson, J. W. McClure and C. Wong, A method for determining scintillator response functions for fast neutrons, UCRL-50653 (1969).
47) H. C. Evans and E. H. Bellamy, Proc. Phys. Soc. (London) **74** (1959) 483.
48) T. J. Gooding and H. G. Pugh, Nucl. Instr. and Meth. **7** (1960) 189.
49) M. Gettner and W. Selove, Rev. Sci. Instr. **31** (1960) 450.
50) M. F. Steuer and B. E. Wenzel, Nucl. Instr. and Meth. **33** (1965) 131.
51) B. Gustafsson and O. Aspelund, Nucl. Instr. and Meth. **48** (1967) 77.

[52]) V. V. Verbinski, J. C. Courtney and N. Betz, Nucl. Instr. and Meth. **52** (1967) 181.
[53]) V. V. Verbinski, W. R. Burrus, T. A. Love, W. Zobel and N. W. Hill, Nucl. Instr. and Meth. **65** (1968) 8.
[54]) T. A. Love and R. J. Schuttler, Measurements of the fast and total light response of NE-213 scintillators to charged particles, ORNL-3714, vol. II (1965) p. 136.
[55]) W. R. Burrus and V. V. Verbinski, Nucl. Instr. and Meth. **67** (1969) 181.
[56]) G. G. Simons and J. M. Larson, Liquid organic fast neutron detector assembly, ANL-7610 (1969) p. 430.
[57]) W. D. Müller, B. Aldefeld and R. Langkau, Nukleonik **11** (1968) 208.
[58]) T. G. Masterson, Nucl. Instr. and Meth. **88** (1970) 61.
[59]) Yu. V. Galaktionov, L. G. Landsberg and V. A. Lyubimov, Nucl. Instr. and Meth. **39** (1966) 351.
[60]) T. Doke, M. Adachi, S. Kubota, M. Tsukuda and E. Tajima, Nucl. Instr. and Meth. **48** (1967) 245.
[61]) D. Bollini, A. Buhler-Broglin, P. Dalpiaz, T. Massam, F. Navach, F. L. Navarria, M. A. Schneegans, F. Zetti and A. Zichichi, Nuovo Cimento **61A** (1969) 125.
[62]) T. T. Dakin, M. G. Hauser, M. N. Kreisler and R. E. Mischke, Performance of a large volume two-phototube neutron detector, PURC-4159-13 (1970).